Analysis and Mitigation of Voltage Offsets in Multi Inverter Microgrids

Shivkumar V. Iyer, Madhu N. Belur and Mukul C. Chandorkar, *Member, IEEE*

***Abstract*—This paper studies microgrids where loads are supplied by parallel connected inverters controlled by decentralized active power/voltage frequency and reactive power/voltage magnitude droop control laws. A paralleled ac system such as a multi-inverter microgrid is susceptible to circulating currents due to differences in voltage magnitude, frequency, phase angle or dc offset. Circulating currents due to differences in voltage magnitude and dc offset have been known issues reported in literature. However, an in-depth analysis of the problem is required to ascertain the deviation of the system operating condition from the desired condition. This paper provides a mathematical model that predicts the effect of voltage magnitude offsets on reactive power sharing between inverters. Simulation and experimental results verify the accuracy of the analytical results obtained from the mathematical model. We examine the effect of dc circulating currents and propose a simple capacitor emulation control law implemented in software to eliminate dc circulating currents. This solution is a possible alternative for hardware implementation to eliminate dc circulating currents. The effectiveness of the capacitor emulation control law has been verified through experimental results.**

***Index Terms*—Microgrids, decentralized control, droop control laws, circulating currents, voltage offsets, capacitor emulation.**

I. Introduction

The parallel connection of dc-ac inverters is an excellent approach towards fabricating large capacity reliable ac power supplies [1]–[13]. This paper considers the case of an ac system comprised of parallel connected inverters supplying associated loads operating in isolation to the main ac grid. This ac system is termed as a microgrid [3]. The parallel connection of inverters that are essentially controlled voltage sources results in a system that is very sensitive to disturbances and offsets. This paper will examine in detail the effect of offsets in the output voltages of the inverters.

To enable inverters to share power demanded by loads in the microgrid according to their maximum capacities, the inverters are controlled to emulate synchronous generators in conventional power systems. The frequency of the output voltage ω is varied as a function of the active power p supplied by the inverters through the p-ω control law. The magnitude of the output voltage V is varied as a function of the reactive power q supplied by the inverters through the q-V droop control law. Voltage controllers are then implemented for the inverter voltages to track the references set by the droop control laws [1]–[13]. The voltage controllers have a high bandwidth and fast dynamics and therefore do not play a significant role in the steady state operating point of the system in comparison to the droop control laws [11], [12].

The circulating currents can originate due to several factors and this paper will discuss them. Detailed examination will be provided to circulating currents due to differences in output voltage magnitudes of the inverters and differences in the dc offsets present in the inverter output voltages. The difference in voltage magnitudes between inverters causes the flow of reactive power between them. Due to the q-V droop control laws, the difference in voltage magnitudes is regulated in such a manner that the inverters share the reactive power demanded by the loads in the microgrid. However, minor fluctuations in the voltage magnitudes will cause the reactive power supplied by the inverters to deviate from the desired values. The sharing of reactive power between the inverters and their output voltage magnitudes will therefore be decided also by the network topology and circuit laws [7], [8], [12], [14].

Another cause of circulating currents is due to a dc offset present in the output voltages of the inverters [13], [15]. These dc offsets may occur due to a measurement offset in the inverter controllers, irregular switching of inverter legs or fluctuations in the dc bus voltage of the inverter [15]. The dc components in the voltages will be limited only by the resistances of the cables and therefore the dc components in the currents between the inverters will be large even for small differences in the dc components in output voltages. The dc current will disrupt the droop control laws by causing large fluctuations in the voltage frequency and magnitude. Moreover, the dc currents will cause additional losses in the microgrid thereby reducing its efficiency. Both software solutions [13] and hardware solutions [15] to eliminate the dc offsets have been found in literature. [13] proposes a method where the dc components in the circulating currents are extracted and fed to a closed loop control that introduces the appropriate dc component in the inverter output voltages. [15] considers the case where the isolating transformer connected at the output of the inverter saturates due to dc offsets in the inverter output voltage. A differential amplifier is designed in hardware that will detect the dc offsets from the positive and negative peaks of the transformer magnetizing current. In the absence of the isolating transformer, the dc offsets in the output voltage can be detected by a saturable reactor connected in the sensing circuit.

The outline of the paper is as follows. Section II provides a basic overview of the origins of circulating currents between voltage sources connected in parallel. Section III describes the topology of the inverter and microgrid. The active and

Shivkumar V. Iyer, Madhu N. Belur and Mukul C. Chandorkar are with the Department of Electrical Engineering of Indian Institute of Technology Bombay, INDIA. Their e-mail IDs are {shivkvi, belur, mukul}@ee.iitb.ac.in.

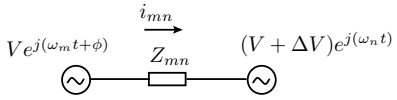

Fig. 1. Power flow between two voltage sources

reactive power flows between inverters are derived. Section IV presents the droop control laws and the application of the q-V droop control law along with the reactive power balance equations in developing a mathematical model. Section V verifies the mathematical model using transient simulations. Section VI provides experimental results for a three inverter ring connected microgrid and a further verification of the reactive power mathematical model. Section VII proposes a controller for eliminating dc offsets from inverter voltages and verifies it by presenting an experimental result.

II. An Examination of Circulating Currents

Fig. 1 shows two voltage sources connected together by a cable. This simple circuit will be used to illustrate the circulating currents that may flow between inverters that are connected by a cable. Fig. 1 shows two voltage sources of angular frequencies ω_m and ω_n and voltage magnitudes V and $(V+\Delta V)$. The voltage sources differ in phase by an angle ϕ.

The current i_{mn} flowing from source m to source n is written as [2]

$$i_{mn} = \frac{Ve^{j(\omega_m t+\phi)} - (V+\Delta V)e^{j(\omega_n t)}}{Z_{mn}} \tag{1}$$

The above equation can be simplified to

$$i_{mn} = \frac{V}{Z_{mn}}e^{j(\omega_n t)}\Big[e^{j[(\omega_m-\omega_n)t+\phi]}-1\Big] - \frac{\Delta V}{Z_{mn}}e^{j(\omega_n t)} \tag{2}$$

The above equation allows us to examine how the circulating current is affected by different factors. The following cases will examine each factor in detail.

A. $\omega_m = \omega_n = \omega$(say), $\Delta V = 0$, $\phi \neq 0$

Substituting the above values in (2), the circulating current is therefore written as

$$i_{mn} = \frac{V}{Z_{mn}}e^{j(\omega t)}\Big[e^{j\phi}-1\Big] \tag{3}$$

For a microgrid, the impedances Z_{mn} of the interconnecting cables will be smaller than the impedances of the transmission lines in conventional power systems. Therefore, the phase angles between voltage sources in a microgrid will be much smaller than that of a power system which leads to the approximation $\cos\phi \approx 1$ and $\sin\phi \approx \phi$. As a result, the circulating current between two voltage sources at the same frequency and without any voltage offset will be small. The smaller the impedance Z_{mn}, the smaller has to be the phase angle difference ϕ and therefore, the design of the droop control laws will have to be done taking into consideration the impedances of the interconnecting cables. Thus the ratio between phase angle differences and cable impedance $\frac{\phi}{Z_{mn}}$ is of importance. It is to be noted that the phase angle difference ϕ between the voltage sources is essential for active power flow.

B. $\omega_m = \omega_n = \omega$(say), $\Delta V \neq 0$, $\phi = 0$

Substituting the above values in (2), the circulating current is therefore written as

$$i_{mn} = -\frac{\Delta V}{Z_{mn}}e^{j(\omega t)} \tag{4}$$

From the above equation, it can be seen that the circulating current originates due to the offset ΔV in the voltage magnitude. If the offsets in the voltage magnitude are chosen to be small with respect to the cable impedances by appropriately designing the q-V droop control laws, the circulating current will therefore be small. As will be shown in the later section, this offset will cause reactive power flow from one voltage source to the other.

C. $\omega_m \neq \omega_n$, $\Delta V = 0$, $\phi = 0$

Substituting the above values in (2), the circulating current is therefore written as

$$i_{mn} = \frac{V}{Z_{mn}}e^{j(\omega_n t)}\Big[e^{j(\omega_m-\omega_n)t}-1\Big] \tag{5}$$

Due to the $[e^{j(\omega_m-\omega_n)t}-1]$ term, the magnitude of the circulating current can attain very large values since the impedance Z_{mn} of the cable is small. Furthermore, the circulating current will have a low frequency envelope of $(\omega_m-\omega_n)$.

D. Dc components in the voltage

For simplicity, the general equation of (2) for circulating currents did not contain a dc component to maintain it to be an equation containing only ac quantities. Before writing the equation for circulating current caused by dc components in the voltages, an important point must be noted with respect to dc voltages. With the assumption that the network is linear, using superposition theorem, the network can be divided into the ac equivalent network and the dc equivalent network. In the dc equivalent network, the dc component of the voltages are limited only by the resistance of the cables during steady state as the inductance of the cable plays no role.

The circulating current can be rewritten considering the dc components as follows

$$\begin{aligned} i_{mn} = {} & \frac{V}{Z_{mn}}e^{j(\omega_n t)}\Big[e^{j[(\omega_m-\omega_n)t+\phi]}-1\Big] - \frac{\Delta V}{Z_{mn}}e^{j(\omega_n t)} \\ & + \frac{v_m^{dc}-v_n^{dc}}{R_{mn}} \end{aligned} \tag{6}$$

The last term in the above equation for circulating current contains the dc component. In microgrids where the inverters are in close proximity, the resistance of the cables can be negligible. Therefore, very small differences in the dc component of the inverter voltages can result in large dc components in the circulating current. In a later section, a solution will be presented to eliminate the dc components in the inverter voltages.

E. Focus of the paper

Four cases have been described above with the expressions of circulating current written in each case. This paper will describe in detail Case B where the magnitudes of the voltage sources differ and Case D where the dc components in the

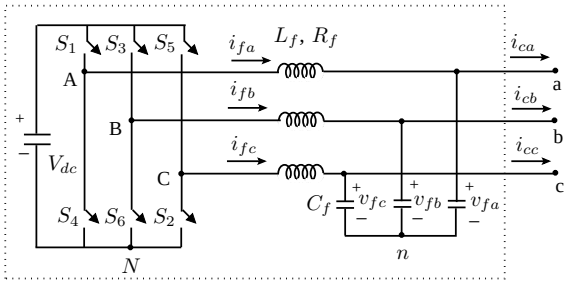

Fig. 2. Topology of the inverters

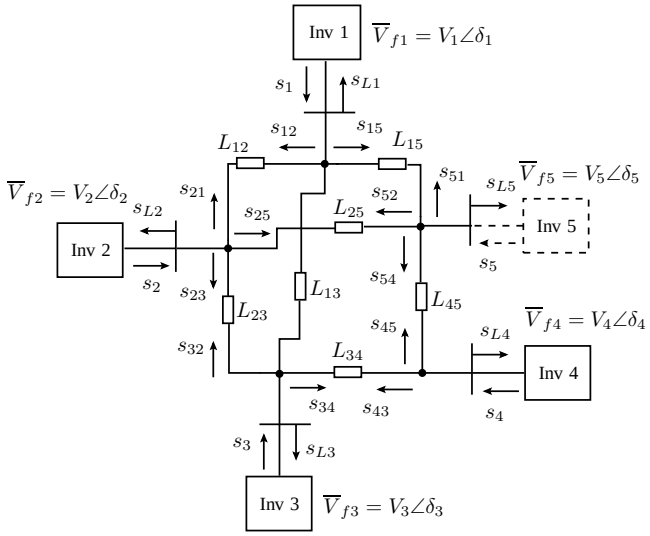

Fig. 3. Microgrid Topology

voltage sources differ. Case A where the voltage sources differ by a phase angle has received detailed treatment in reported literature. Case C where the voltage sources have different frequencies has been proved to be an unacceptable operating condition which in turn laid the foundation for p-ω droops.

III. System Topology and Power Flow Equations

This section will begin with a description of the inverter topology and the topology of the microgrid chosen for analysis and simulation study. The topology of the microgrid used for hardware verification will be provided in a later section. In the topologies of the three phase microgrid and the three phase inverter, parameters are assumed to be equal in all phases without any mutual coupling between the phases. Moreover, the entire three phase system is assumed to be a three wire system without a neutral wire.

Fig. 2 shows the topology of the three phase three wire inverter. The energy source for the inverter has been assumed to be a constant voltage source V_{dc}. In practice, this would be either be the output of a rectifier fed by an ac supply or an alternative energy source such as a microturbine, diesel generator, photovoltaic panel, fuel cell etc. The switches S_1 to S_6 are Insulated Gate Bipolar Transistors (IGBTs) with their associated anti-parallel diodes. The inductor L_f and the capacitor C_f form a low pass L-C filter. The voltages v_{fa}, v_{fb}, v_{fc} across the filter capacitor bank C_f are the output voltages of the inverter. Details about the design and control of the inverter of the topology of Fig. 2 can be found in [16].

Fig. 3 is a single line diagram showing the topology of a three phase four inverter meshed microgrid. The topology of Fig. 3 has been selected for analysis and simulation as it presents a microgrid with sufficient complexity. However, the experimental results will be presented for a simpler microgrid. In the figure, the load at bus 5 is a remote load not supported locally by a inverter. Therefore, an inverter (Inverter 5) is shown in dotted lines. This inverter is a fictitious inverter which will be included in the mathematical model to examine the case of a remote load connected at a bus not supported by a inverter. The significance of a fictitious inverter will be discussed after the mathematical model of the microgrid has been derived. In the discussion below, Inverter 5 will be assumed to be a real inverter and the microgrid will be assumed to be a five inverter microgrid.

L_{12}, L_{23}, L_{34}, L_{45}, L_{13}, L_{15}, L_{25} are the inductances of the interconnecting cables between the inverters with the resistances of the cables being neglected. Fig. 3 also shows the power flowing in the interconnecting cables between the inverters. The terminology used for the power flowing between inverters is described taking the interconnection between Inverter 1 and Inverter 2 as an example. $s_{12} = p_{12} + jq_{12}$ is the complex power flowing in the cable connecting Inverter 1 and Inverter 2 with p_{12} and q_{12} being the active and reactive power flow respectively. s_1, s_2, s_3, s_4 and s_5 are the complex powers supplied by the inverters. s_{L1}, s_{L2}, s_{L3}, s_{L4} and s_{L5} are the complex power demanded by the loads connected locally to the five inverters. For analysis, these loads are assumed to be linear, balanced three phase loads.

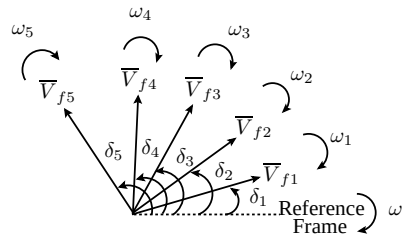

Fig. 4. Voltage vectors

Fig. 3 shows the output voltages vectors of the inverters as complex quantities in polar form. The output voltages of the inverters shown are $\overline{V}_{f1} = V_1\angle\delta_1$, $\overline{V}_{f2} = V_2\angle\delta_2$, $\overline{V}_{f3} = V_3\angle\delta_3$, $\overline{V}_{f4} = V_4\angle\delta_4$, $\overline{V}_{f5} = V_5\angle\delta_5$. The magnitudes V_1, V_2, V_3, V_4, V_5 are assumed to be the Root-Mean-Squared (R.M.S) values of the line-to-neutral output voltages. The angles δ_1, δ_2, δ_3, δ_4, δ_5 are measured with respect to an arbitrary reference frame and in the figure are shown in an arbitrary manner. The voltage vectors $\overline{V}_{f1}$, $\overline{V}_{f2}$, $\overline{V}_{f3}$, $\overline{V}_{f4}$, $\overline{V}_{f5}$ are rotating with angular frequencies of ω_1, ω_2, ω_3, ω_4, ω_5 respectively. The reference frame is rotating with an angular frequency of ω. However, at steady state $\omega_1 = \omega_2 = \omega_3 = \omega_4 = \omega_5 = \omega$, *i.e* all the vectors and the reference frame are rotating with the same angular frequency. It is to be noted that the vector diagram of Fig. 3 is only for the purpose of deriving the mathematical model below. In reality, the phase

angle differences between the voltage vectors will be very small and the sequence of the vectors will depend on the active power demanded by the loads in the microgrid.

The assumptions necessary for the subsequent analysis to follow will be listed below:

1) The microgrid has been assumed to be a three phase balanced system with all loads being three phase balanced loads and network parameters being equal in all three phases.
2) The resistance of the feeders are negligible as compared to the inductive reactances and therefore have been neglected.
3) The microgrid has been assumed to cover a small area and therefore the cable impedances are small. As a result, a small phase angle difference and voltage magnitude difference required to cause active and reactive power flow between the inverters.
4) The p-ω droop control laws produce a steady state deviation in frequency up to 1% of the nominal frequency while the q-V droop control laws produce a state deviation in voltage magnitude up to 2-4% of the nominal voltage magnitude of the microgrid.
5) The internal dynamics of the inverter are neglected since the voltage controllers proposed in [16] have a high bandwidth with fast transient responses. The inverters are therefore assumed to be ideal voltage sources that are exactly equal to the references set by the droop control laws [11], [12].

It is to be noted that the assumption of balanced three phase three wire system is important. In such a balanced three phase system, the power flows marked in Fig. 3 will be constant values at steady state. However, if the system is unbalanced due to inequality of the line inductances in the three phases or due to the connection of unbalanced or non-linear load, the power flows will not be constant values at steady state.

Fig. 3 shows the power flows between the five inverters. The expression for the power flow from any Inverter m towards another Inverter n is given by

$$\begin{aligned} p_{mn} &= \frac{3V_mV_n}{\omega L_{mn}}\sin\delta_{mn} \approx \frac{3V_mV_n}{\omega L_{mn}}\delta_{mn} \\ q_{mn} &= \frac{3V_m(V_m - V_n\cos\delta_{mn})}{\omega L_{mn}} \approx \frac{3V_m(V_m - V_n)}{\omega L_{mn}} \end{aligned} \tag{7}$$

In a microgrid, the impedances of the interconnecting cables is low as the distances between inverters is significantly lesser than of a conventional transmission system. Therefore, for a particular flow of power through a cable, the phase angle difference $\delta_{mn} = \delta_m - \delta_n$ between inverters is small. In the above equation, the approximation of $\sin\delta_{mn} \approx \delta_{mn}$ and $\cos\delta_{mn} \approx 1$ is valid [2].

From (7), it can be observed that the active power flow p_{mn} depends to a large extent on the phase angle difference δ_{mn} while the reactive power flow q_{mn} depends to a large extent on the voltage magnitude difference $V_m - V_n$. Therefore, the active power and reactive power flowing between inverters can be controlled by controlling the phase angle difference and voltage magnitude difference of the inverters respectively. The phase angle difference is controlled by controlling the frequency of the output voltages of the inverters. This is the underlying principle behind the droop control strategy that will be analyzed in this paper.

IV. Reactive Power Sharing and Voltage Magnitude Profile

The droop control strategy consists of two droop laws. The droop controller is applied to every inverter in the microgrid and it requires the measurement of variables local to the inverter. The droop controller laws for Inverter m are written as [1]–[13]

$$\begin{aligned} \omega_m &= \omega_0 - k_{pm}p_m \\ V_m &= V_0 - k_{qm}q_m \end{aligned} \tag{8}$$

where ω_0 and V_0 are the nominal angular frequency and voltage magnitude for the microgrid while ω_m and V_m are the angular frequency and output voltage magnitude of Inverter m. k_{pm} and k_{qm} are the p-ω and q-V droop control gains of Inverter m respectively. In the analysis below, the q-V droop control law will be analyzed in detail. A further approximation can be made to the reactive power flow equation in (7). The q-V droop control law of (8) produces a droop in the inverter output voltage magnitude upto 2-4% of the nominal voltage to ensure that voltage regulation in the microgrid remains acceptable. Therefore, the reactive power flowing from Inverter m to Inverter n is written as

$$q_{mn} \approx \frac{3V_0(V_m - V_n)}{\omega L_{mn}} \tag{9}$$

where the magnitude of Inverter m output voltage V_m has been approximated to the nominal voltage magnitude V_0.

The reactive power balance equation at each inverter is written as follows

$$\begin{aligned} q_1 &= q_{12} + q_{13} + q_{15} + q_{L1} \\ q_2 &= q_{21} + q_{23} + q_{25} + q_{L2} \\ q_3 &= q_{31} + q_{32} + q_{31} + q_{L3} \\ q_4 &= q_{43} + q_{45} + q_{L4} \\ q_5 &= q_{51} + q_{52} + q_{54} + q_{L5} \end{aligned} \tag{10}$$

By substituting (9) and (8) into (10) and suitably rearranging the equation, the following matrix equation is obtained

$$\Big(I + \frac{3V_0}{\omega}\,\mathbf{A}_q\,\mathbf{A}_k\Big)\mathbf{q} = \mathbf{q}_L \tag{11}$$

where

$$\begin{aligned} \mathbf{A}_k &= \mathrm{diag}(k_{q1}, k_{q2}, k_{q3}, k_{q4}, k_{q5}) \\ \mathbf{q} &= [q_1 \;\; q_2 \;\; q_3 \;\; q_4 \;\; q_5]^T \\ \mathbf{q}_L &= [q_{L1} \;\; q_{L2} \;\; q_{L3} \;\; q_{L4} \;\; q_{L5}]^T \end{aligned}$$

and

$$\mathbf{A}_q = \begin{bmatrix} d_{12}+d_{13}+d_{15} & -d_{12} & -d_{13} & 0 & -d_{15} \\ -d_{12} & d_{12}+d_{23}+d_{25} & -d_{23} & 0 & -d_{25} \\ -d_{13} & -d_{23} & d_{13}+d_{23}+d_{34} & -d_{34} & 0 \\ 0 & 0 & -d_{34} & d_{34}+d_{45} & -d_{45} \\ -d_{15} & -d_{25} & 0 & -d_{45} & d_{15}+d_{25}+d_{45} \end{bmatrix} \tag{12}$$

In the matrix $\mathbf{A}_q$, the coefficient $d_{mn} = 1/L_{mn}$.

The above matrix equation of (11) provides a method of designing the droop control gains of the inverters. The above matrix equation can be simplified to the following form:

$$\mathbf{A}_q \, \mathbf{A}_k \, \mathbf{q} = \frac{\omega}{3V_0}\Big(\mathbf{q}_L - \mathbf{q}\Big) \tag{13}$$

The q-ω droop control gains in matrix $\mathbf{A}_k$ can be designed so that the inverters share the reactive power demanded by the loads $\mathbf{q}_L$ in a desired manner namely $\mathbf{q}$. Equation (13) can be compared with the standard matrix equation $\mathbf{Ax} = \mathbf{b}$ where $\mathbf{A} = \mathbf{A}_q$, $\mathbf{x} = \mathbf{A}_k\mathbf{q}$ and $\mathbf{b} = \frac{\omega}{3V_0}(\mathbf{q}_L - \mathbf{q})$. From an inspection of the matrix $\mathbf{A}_q$ in (12), it can be observed that the rows and columns of $\mathbf{A}_q$ add up to zero. This property of the matrix $\mathbf{A}_q$ will hold good for any arbitrary microgrid due to the mathematical model being formulated from the reactive power balance laws. Hence matrix $\mathbf{A}_q$ turns out to be singular. Therefore, a solution for (13) will exist when the rows of $(\mathbf{q}_L - \mathbf{q})$ add up to zero. Moreover, a unique solution to the matrix equation will not exist due to the singularity of $\mathbf{A}_q$. The inverters can share reactive power in a non unique manner similar to the sharing of active power due to the p-ω droop control laws where the ratio of the p-ω droop control gains are what matter.

The stability of the microgrid with respect to the q-V droop control law is examined by an alternative matrix equation derived from (8), (9) and (10). Substituting the reactive power flow equation in (7) into (10) and then substituting the resulting equation into the q-V droop control law in (8), the following matrix equation can be obtained.

$$\Big(\mathbf{I} + \frac{3V_0}{\omega}\mathbf{A}_k \, \mathbf{A}_q\Big)\mathbf{V} + \mathbf{A}_k \, \mathbf{q}_L = \mathbf{V}_0 \tag{14}$$

where

$$\mathbf{V} = [V_1 \;\; V_2 \;\; V_3 \;\; V_4 \;\; V_5]^T$$
$$\mathbf{V}_0 = [V_0 \;\; V_0 \;\; V_0 \;\; V_0 \;\; V_0]^T$$

Equation (14) does not contain any dynamics *i.e* the $\frac{d}{dt}(V)$ is absent. Therefore, for a finite deviation in the reactive power demand of the load and for finite values of q-V droop control gains, the microgrid will always be stable. However, the q-V droop law will not result in the reactive power demand of the loads to be shared in accordance with the droop control gains since the voltage magnitudes of the inverters are constrained by network parameters and network topology. The matrix equation of (11) can be used to compute the reactive power supplied by the inverters for the reactive power demand of the load as will be shown soon.

The above discussions have provided us with the following proofs with which the case of a remote load can be considered. In the mathematical models of (14), instability of the microgrid does not occur for any non-zero finite value of the q-V droop control gain k_q. With reference to the microgrid topology of Fig. 3, let us assume that Inverter 5 does not exist and that only a load is connected at that bus drawing a reactive power of q_{L5}. The mathematical models of (14) and (11) assume that every load in the microgrid is local to an inverter. To continue using these models, we consider a fictitious inverter (Inverter 5) at the remote load. This inverter should supply a negligible amount of reactive power so as to capture the behavior of the microgrid with the remaining four inverters.

The droop control gain k_{q5} of Inverter 5 is designed as follows. At steady state, the voltage magnitudes of the inverters will be approximately equal. Therefore, the following equation is written for steady state

$$n_1 q_1 = n_2 q_2 = \ldots = n_5 q_5 \tag{15}$$

From the above equation it is evident that in order to make the reactive power contribution q_5 of Inverter 5 to be negligible with respect to the other inverters, the droop control gain k_{q5} is made much larger than the other inverters. For example, if the droop control gain k_{q5} is made 100 times larger than the control gains of other inverters, q_5 should be approximately 1% of the contributions of other inverters. In the next section which validates the model of (11), this design criterion will be used.

V. Reactive power contribution of Inverters

Equation (11) provides a method to calculate the change in the reactive power supplied by the inverters for a change in the reactive power demanded by the loads in the microgrid. Two methods are used to validate the expression. In this subsection, the expression will be verified by comparing it with a complete transient simulation of the four inverter meshed microgrid of Fig. 3 performed in C++. In the next section, the expression of (11) will be verified by experimental results on a three inverter ring connected microgrid.

TABLE II
Inductances of Interconnecting Cables

$L_{12} = L_{23} = L_{34} = L_{13} = 150\mu$ H
$L_{45} = 200\mu$ H, $L_{51} = 250\mu$ H, $L_{25} = 450\mu$ H

TABLE III
Base System Parameters

Base kVA = 5, V_{base} = 400 V (L-L)
L_{base} = 0.101 H, Base ω = 100 π rad/s

Table II lists the inductances of the interconnecting cables between the inverters as shown in Fig. 3. The stability of the system is examined with all the parameters in per unit (p.u). Therefore, a base system has been chosen with respect to which all the p.u values of the chosen system are calculated. Table III lists the parameters of the base system.

In the transient simulation in C++, the loads connected at the buses are considered to be balanced resistive-inductive loads that draw active and reactive power. Different values of the load resistance and inductance are chosen such different cases are generated and the reactive power demanded by the loads is recorded. Subsequently, the reactive power supplied by the inverters is also recorded. The reactive power demanded by the loads obtained from the transient simulation are fed to model of (11) and the analytical values of the reactive power supplied by the inverters are calculated.

The results of the simulation study are listed in Table I. Five different cases of loading have been considered as shown in

TABLE I
CHANGE IN REACTIVE POWER SUPPLIED BY INVERTERS FOR $k_{q1} = k_{q2} = k_{q3} = k_{q4} = k_{q5} = 0.021$ P.U

		$q_{L1} = 0.253$ $q_{L2} = 0.337$ $q_{L3} = 0.253$ $q_{L4} = 0.253$ $q_{L5} = 0.202$	$q_{L1} = 0.33$ $q_{L2} = 0.33$ $q_{L3} = 0.99$ $q_{L4} = 0.25$ $q_{L5} = 0.25$	$q_{L1} = 0.986$ $q_{L2} = 0.329$ $q_{L3} = 0.493$ $q_{L4} = 0.246$ $q_{L5} = 0.985$	$q_{L1} = 0.9806$ $q_{L2} = 0.3217$ $q_{L3} = 0.981$ $q_{L4} = 0.2453$ $q_{L5} = 0.9792$	$q_{L1} = 0.969$ $q_{L2} = 0.969$ $q_{L3} = 0.485$ $q_{L4} = 0.969$ $q_{L5} = 0.967$
q_1	Simulation	0.3254	0.5417	0.7772	0.8943	1.101
	Numerical	0.3237	0.5395	0.7628	0.8795	1.088
	Error %	0.51%	0.41%	1.93%	1.68%	1.21%
q_2	Simulation	0.3263	0.541	0.7620	0.8788	1.098
	Numerical	0.3231	0.5392	0.7576	0.8743	1.087
	Error %	0.69%	0.31%	0.67%	0.51%	1.05%
q_3	Simulation	0.324	0.551	0.7608	0.8857	1.0839
	Numerical	0.3233	0.5426	0.7572	0.8767	1.088
	Error %	0.2%	1.54%	0.47%	1.03%	0.40%
q_4	Simulation	0.3253	0.54	0.7600	0.8772	1.106
	Numerical	0.3238	0.5388	0.7571	0.8738	1.089
	Error %	0.47%	0.22%	0.38%	0.38%	1.51%

Table I. The first case considers the microgrid to be lightly loaded with the reactive power demanded by the loads in the microgrid being less than 0.5 p.u. The remaining cases consider heavier loads ($>$ 0.8 p.u) connected at one or more bus. Finally, the fifth case considers a heavily loaded microgrid where only one load draws a reactive power less than 0.5 p.u. The results in Table I contain results from the C++ simulation, analytical results obtained from substituting change in reactive power demand into (11) and the percentage error between them calculated as follows

$$\%\text{Error} = \frac{q_{i(\text{sim})} - q_{i(\text{anal})}}{q_{i(\text{sim})}} \times 100 \tag{16}$$

As can be seen from Table I, a close agreement exists between the C++ simulations and the analytical results obtained from the reactive power model of (11). The highest percentage error encountered in the study is 1.93%. Therefore, the simulation results validate the reactive power model of (11). As a final confirmation, the next section will present experimental results.

VI. EXPERIMENTAL RESULTS

The microgrid topology chosen for experimental verification is a three inverter ring connected microgrid shown in Fig. 5. Each inverter has a local load: Z_{L1}, Z_{L2}, Z_{L3} for Inverter 1, Inverter 2, Inverter 3 respectively. The inverters are connected to their local loads directly but are connected to the microgrid through contactors K1, K2, and K3 controlled by synchronizing circuits. The synchronizing circuit closes an ac contactor when the output voltage of the inverter is in phase with the microgrid voltage at the point of connection thereby reducing transients at the moment of inverter interconnection.

Table IV lists the parameters of the inverters whose topology has been shown in Fig. 2. The L_f-C_f filter parameters have been chosen so as provide a resonant frequency of 205 Hz. As also listed in Table IV, the Pulse Width Modulation (PWM) switching frequency of the inverter is 5 kHz. Therefore, as will be shown in the experimental results, the high

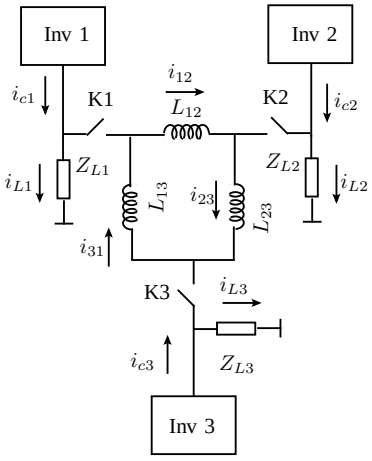

Fig. 5. Experimental setup of the Microgrid

TABLE IV
PARAMETERS OF THE INVERTERS

Inverter
Dc bus voltage = 250 V, Switching frequency = 5 kHz
$L_f = 3$ mH, 25A, $L_c = 400\mu$H, 25A, $C_f = 200\mu$F, 440V
Inductances emulating interconnecting cables
$L_{12} = 150\mu$H, $L_{23} = 150\mu$H, $L_{13} = 200\mu$H

frequency switching harmonics are sufficiently attenuated so as to produce smooth sinusoidal waveforms. Another additional inductor L_c has been listed in Table IV. This inductor L_c is an interfacing inductor that is connected at the output of the inverter. This inductor reduces the effects of transients in the microgrid such as the interconnection or disconnection of another inverter. However, this inductor has been limited in size to ensure that the transient response of the inverter is not adversely affected.

Table V lists the details of the loads Z_{L1}, Z_{L2}, Z_{L3}. Z_{L1} consists of a resistive lamp load drawing only active power and a reactor that draws reactive power. Z_{L2} and Z_{L3} are purely resistive lamp loads drawing only active power. The

TABLE V
DETAILS OF LOADS

Z_{L1}	Resistive load of six 250V, 200W incandescent lamps. Tunable inductor load of 22 mH, 25A
Z_{L2}	Resistive load of four 250V, 200W incandescent lamps.
Z_{L3}	Resistive load of six 250V, 200W incandescent lamps.

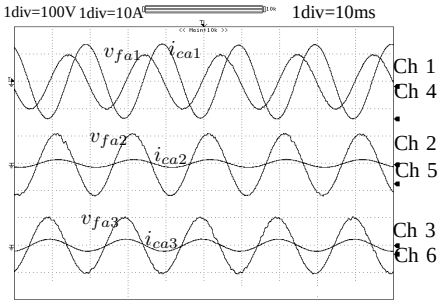

Fig. 6. Standalone operation of inverters

nominal angular frequency and voltage magnitude are chosen as $\omega_0 = 100\pi$ rad/s and $V_0 = 85$ V. The droop control gains of the inverters are chosen to be equal with $k_{p1} = k_{p2} = k_{p3} = 0.0125$ rad/(W-s) and $k_{q1} = k_{q2} = k_{q3} = 10^{-3}$ V/VAR. With respect to the theory presented in Section III, the active power should be shared equally as the frequency of all inverters have to be equal in steady state. However, the reactive power will be shared according to (11). In this experiment, the reactors are not turned on or off to produce a transient. However, the inverters can be connected to the microgrid through the contactors K1, K2, K3. Therefore, initially the inverters will operate in standalone mode supplying the load local to them and by closing K1, K2 and K3, these will be brought in parallel to form the microgrid. With only load Z_{L1} demanding reactive power, this will be equivalent to q_{L1} being non-zero while the others q_{L2}, q_{L3} are zero.

The standalone operation of the inverters where they are feeding their own local loads is shown in Fig. 6. The phase a output voltages and output currents of the inverters are plotted together with one common scale for the voltages and another common scale for the currents. As can be seen from the figure, the load local to Inverter 1 draws a current much larger as compared to the loads local to Inverter 2 and Inverter 3. This is due to the fact that the entire reactive power load is concentrated near Inverter 1. Upon parallel operation of the inverters to form a microgid, it is expected that the currents will be of approximately equal magnitude. Fig. 7 shows the phase a output voltages of the inverters when the contactors K1, K2 and K3 are closed and the microgrid has been formed. As can be observed, the inverter output voltages have equal magnitudes and have almost unnoticeable phase differences between them.

Fig. 8 shows the phase a output currents of the three inverters. As can be seen from the figure, the currents are approximately in phase with the magnitudes of Inverter 2 and Inverter 3 output currents being approximately equal. However, the output current of Inverter 1 is larger than that of Inverter 2 and Inverter 3. The reason for this difference

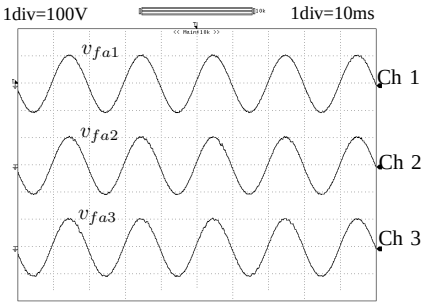

Fig. 7. Phase a output voltages of inverters when connected to microgrid

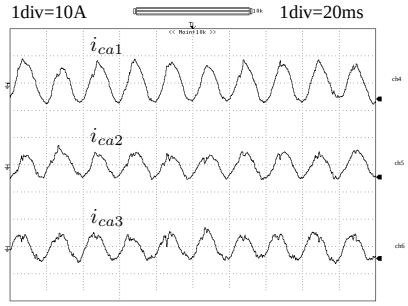

Fig. 8. Phase a output currents of inverters when connected to microgrid

lies in the fact that the reactive power load is concentrated at Inverter 1. As stated previously, the active power supplied by all inverters will be equal as the p-ω droop control gains are equal for all inverters. However, despite the q-V droop control gains being equal, the reactive power supplied by the inverters will not be equal as the output voltage magnitudes of the inverters are constrained by the network laws. This will be evident from the plots of the powers supplied by the inverters.

The reactive power demanded by the three phase load reactor is 2200 VAR at the nominal line-to-neutral voltage $V_0 = 85$ V. Upon substitution of $q_{L1} = 2200$ VAR, $q_{L2} = 0$, $q_{L3} = 0$ in (11), the reactive power supplied by the inverters are computed to be $q_1 = 900.85$ VAR, $q_2 = 659.35$ VAR, $q_3 = 639.79$ VAR. Fig. 9(b) shows the reactive power supplied by the inverters. As expected, the reactive power supplied is not equal as the voltage profiles are dependent on the network topology. Comparing the experimental results of the reactive powers supplied by the inverters with the numerical values obtained from (11), the error is found to be negligible. The difference in the reactive power obtained with respect to (11) can be attributed to the approximations made in obtaining (11) and in the errors and offsets in the measurement of voltages and currents in the experimental setup. Fig. 9(a) shows the three inverters sharing the active power demanded by the loads in the microgrid equally as expected.

VII. CORRECTION OF DC OFFSET

Section II described the origin of dc circulating currents due to dc components in the inverter output voltages. The dc components appear in the inverter output voltages due to offsets generated in the conditioning of the measured signals by circuits based on OPerational AMPlifiers (OPAMPs). These signal conditioning circuits are essential when the input to the

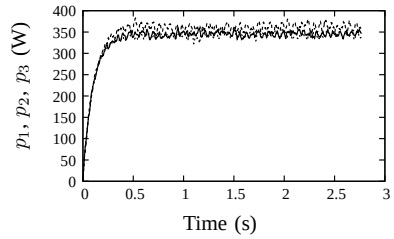

(a) Active power supplied by the inverters

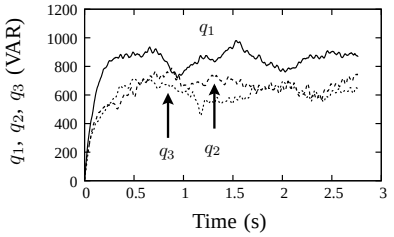

(b) Reactive power supplied by the inverters

Fig. 9. Active and reactive power supplied by the inverters

Analog to Digital Converter (ADC) is unipolar; for example - 0 to 5V. As a result, the measured signals have to be attenuated and level shifted. These processes produce a dc offset in the signals fed to the ADC. Moreover, the dc offset varies with temperature, drift of parametric values of electronic components etc. Other causes for a dc offset to appear in the output voltage are the switching delays in the two IGBTs of inverter legs and fluctuations in the dc bus voltage of the inverter.

This section will describe a method to eliminate dc offsets based on a fundamental network property. An ac capacitor connected in series with the circuit has the property of blocking dc current from flowing in the circuit. This is due to the ac capacitor in effect offering a very large impedance to dc. Connecting an ac capacitor at the output of the inverter is not desirable due to the increased bulk of the inverter. The ac capacitor is therefore emulated in the controller as will be described below. This emulation also provides a flexibility in changing the value of the capacitor by merely changing the code in the DSP processor.

If the desired ac voltage as set by the droop control laws is v_{fref}, then we denote the desired inverter output voltage with ac capacitor emulation by v_{oref}. The emulator control law is written as

$$v_{oref} = v_{fref} - \frac{1}{C_{out}} \int i_c dt \tag{17}$$

where C_{out} is the emulated ac capacitor. The effect of the above controller can be examined with respect to an example. Assume the inverter output current i_c to have the following components

$$i_c = I_{dc} + I_{c1} \sin(\omega t) + I_{c3} \sin(3\omega t) + I_{c5} \sin(5\omega t) \tag{18}$$

The integral of the above current will provide the following expression with initial conditions being neglected

$$\int i_c dt = I_{dc} t + \frac{I_{c1}}{\omega} \cos(\omega t) + \frac{I_{c3}}{3\omega} \cos(3\omega t) + \frac{I_{c5}}{5\omega} \cos(5\omega t) \tag{19}$$

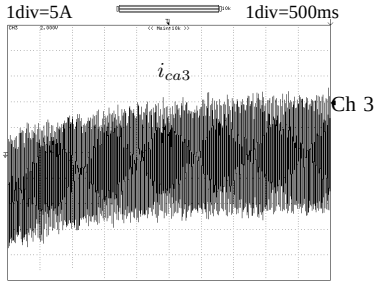

Fig. 10. Dc offset correction in phase a output currents of Inverter 3

In the above equation, the angular frequency $\omega \approx 100\pi$ rad/s. The contribution of the above integral with respect to fundamental and higher harmonics will be negligible. However, the contribution due to the dc component of current I_{dc} will be a dc component continuously increasing with time. The $\frac{1}{C_{out}}$ in the controller equation (17) can be interpreted as a gain constant.

The operation of the controller is as follows. A positive dc offset I_{dc} in the current i_c will be due to the presence of a dc offset in the inverter output voltage that is larger than the dc offsets in other inverter voltages. Due to the control law of (17), the desired inverter output voltages will contain a dc offset that decreases with time. The decrease in the dc offset in the inverter output voltage causes the dc offset in the inverter output current i_c to decrease. At steady state, the dc offset in the output voltages of all the inverter units will be equal and the dc offsets in the inverter output currents will be zero.

The capacitor emulation law of (17) has been implemented in DSP and is associated with every inverter in the microgrid. A virtual series capacitor of 100 millifarad has been emulated in DSP. The effect of the controller is best seen at the moment of interconnection of a inverter to a microgrid. Fig. 10 shows the output current in phase a of Inverter 3 when it is connected to a microgrid with Inverter 1 and Inverter 2 already operating in parallel. As can be seen from Fig. 10, immediately following the interconnection of Inverter 3, a large negative dc offset can be seen in the current i_{ca3}. As time progresses, the dc offset decreases and finally becomes zero. The time taken to eliminate the dc offset in the output current can be varied by changing the capacitor C_{out} emulated in (17).

The value of the capacitor chosen for the above case is such that the capacitive reactance is small and does not disturb the predominantly inductive nature of the microgrid. This can be observed from the slow decay of the dc component in the inverter output current. The value of the capacitor can be decreased so as to increase the capacitive reactance at fundamental frequency (50 Hz). This might result in faster transients where the dc components will be eliminated faster as seen from (17). However, larger capacitive reactances due to smaller emulated capacitances may result in stability issues due to resonance with the inductances of the interconnecting cables. Therefore, if fast transients are desired, stability analysis is required to obtain the lower limit of capacitance that can be emulated.

VIII. Conclusions

The paper has provided a detailed analysis of the origin of circulating currents leading to imperfect sharing of reactive power by inverters and dc circulating currents. The issue of imperfect sharing of reactive power by inverters has been addressed in literature. However, a model to predict the nature in which load reactive power demand will be shared has not been proposed in literature. Such a model is essential to understand the extent of the problem with respect to micogrid topologies and q-V droop control gains. The paper has proposed a mathematical model that can be written by mere inspection of the microgrid topology and a knowledge of the interconnecting cable inductances. This model can also be used to design the q-V droop control gains if the reactive power to be shared between inverters is known for a given load demand profile. The effectiveness of the model has been verified through simulations and experimental results.

The presence of dc circulating currents can disrupt the operation of the microgrid due to very large current flows that may lead to nuisance tripping. Moreover, dc circulating currents are generated due to dc offsets in inverter voltages that vary with electronic components values, noise etc. As a result, a microgrid may become susceptible to dc circulating currents at a later stage due to component ageing. The paper has proposed a simple and computationally light controller to eliminate dc circulating currents. The effectiveness of the controller has been shown through experimental results.

Acknowledgements

This work was supported in part by the SERC Division, Department of Science and Technology.

References

[1] M. Chandorkar, D. Divan, and R. Adapa, "Control of parallel connected inverters in standalone ac supply systems," *IEEE Transactions on Industrial Applications*, vol. 29, no. 1, pp. 136–143, January/February 1993.

[2] M. Chandorkar, "Distributed uninterruptible power supply systems," Ph.D. dissertation, University of Wisconsin-Madison, October 1995.

[3] R. Lasseter and P. Piagi, "Microgrids : A conceptual solution," in *35th Power Electronics Specialists Conference*, vol. 6, June 2004, pp. 4285–4290.

[4] U. Borup, F. Blaabjerg, and P. Enjeti, "Sharing of nonlinear load in parallel-connected three-phase converters," *IEEE Transactions on Industry Applications*, vol. 37, no. 6, pp. 1817–1823, November/December 2001.

[5] E. Coelho, P. Cortizo, and P. Garcia, "Small-signal stability for parallel-connected inverters in stand-alone ac supply systems," *IEEE Transactions on Industrial Applications*, vol. 38, no. 2, pp. 533–542, March/April 2002.

[6] P. Strauss and A. Engler, "Ac coupled pv hybrid systems and micro grids : state of the art and future trends," in *3rd World Conference on Photovoltaic Energy Conversion*, vol. 3, May 2003, pp. 2129–2134.

[7] C. Sao and P. Lehn, "Autonomous load sharing of voltage source converters," *IEEE Transactions on Power Delivery*, vol. 20, no. 2, pp. 1009–1016, April 2005.

[8] J. Guerrero, L. Vicuna, J. Matas, M. Castilla, and J. Miret, "Output impedance design of parallel-connected ups inverters with wireless load-sharing control," *IEEE Transactions on Industrial Electronics*, vol. 52, no. 4, pp. 1126–1135, August 2005.

[9] N. Pogaku, N. Prodanovic, and T. Green, "Modeling, analysis and testing of autonoumous operation of an inverter-based microgrid," *IEEE Transactions on Power Electronics*, vol. 22, no. 2, pp. 613–625, March 2007.

[10] J. Guerrero, L. Hang, and J. Uceda, "Control of distributed uninterruptible power supply systems," *IEEE Transactions on Industrial Electronics*, vol. 55, no. 8, pp. 2845–2859, August 2008.

[11] E. Barklund, N. Pogaku, M. Prodanovic, C. Aramburo, and T. Green, "Energy management in autonomous microgrid using stability-constrained droop control of inverters," *IEEE Transactions on Power Electronics*, vol. 23, no. 5, pp. 2346–2352, September 2008.

[12] Y. Mohamed and E. Saadany, "Adaptive decentralized droop controller to preserve power sharing stability of paralleled inverters in distributed generation microgrids," *IEEE Transactions on Power Electronics*, vol. 23, no. 6, pp. 2806–2816, November 2008.

[13] M. Xie, Y. Li, K. Cai, P. Wang, and X. Sheng, "A novel controller for parallel operation of inverters based on decomposing of output current," in *Industrial Applications Society General meeting*, vol. 22, October 2005, pp. 1671–1676.

[14] J. Guerrero, L. Vicuna, J. Matas, M. Castilla, and J. Miret, "Wireless-control strategy for parallel operation of distributed-generation inverters," *IEEE Transactions on Industrial Electronics*, vol. 53, no. 5, pp. 1461–1470, October 2006.

[15] B. R. Rhodes and D. W. Jodlowski, "Inverter power supply system," Patent US 4,939,633, July 13, 1990.

[16] P. Loh, M. Newman, D. Zmood, and D. Holmes, "A comparative analysis of multiloop voltage regulation strategies for single and three-phase ups systems," *IEEE Transactions on Power Electronics*, vol. 18, no. 5, pp. 1176–1185, September 2003.

Shivkumar V. Iyer completed his Bachelor of Engineering from Electrical Engineering in 2002 from Mumbai University and Master of Technology in 2004 from Indian Institute of Technology Kanpur. He is pursuing his Ph.D from Indian Institute of Technology Bombay in Electrical Engineering. At present, he is an Associate Scientist at ABB Global Industries and Services Ltd, Bangalore. His research interests are power electronics and decentralized control of modular systems.

Madhu N. Belur finished Bachelor in Mechanical Engineering from Indian Institute of Technology Bombay in the year 1997, and Ph.D. in Systems Theory, from Institute for Mathematics and Computing Science, University of Groningen, the Netherlands in the year 2003. He is an Assistant Professor since 2003 in the Department of Electrical Engineering, Indian Institute of Technology Bombay. He works in control theory, in particular, dissipative systems, impulse free interconnection of dynamical systems and graph theoretic methods in control.

Mukul C. Chandorkar (M84) received the B.Tech. degree from Indian Institute of Technology, Bombay, India, the M. Tech. degree from Indian Institute of Technology, Madras, India, and the Ph.D. degree from the University of Wisconsin, Madison, in 1984, 1987, and 1995, respectively, all in electrical engineering. He has several years of experience in the power electronics industry in India, Europe, and the U.S. During 1996-1999, he was with ABB Corporate Research Ltd., Baden- Dattwil, Switzerland. He is currently a Professor in the Electrical Engineering Department, Indian Institute of Technology, Mumbai, India. His technical interests include uninterruptible power supplies, drives, real-time simulation of power electronic systems, and the measurement and analysis of power quality.